

Article

Research on Bonding Performance of Anchorage Caisson Foundation with Different Contact Surfaces and Grouting Bed

Tiesuo Geng ^{1,*}, Shuanghua Chen ², Liuqun Zhao ² and Zhe Zhang ¹¹ School of Civil Engineering, Dalian University of Technology, Dalian 116024, China; zhangzhe@dlut.edu.cn² The Second Engineering Company of CCCC Fourth Harbor Engineering Co. Ltd., Guangzhou 510230, China; cshuanghua@cccc4.com (S.C.); zliuqun@cccc4.com (L.Z.)

* Correspondence: gengts@dlut.edu.cn

Abstract: In view of the first domestic offshore suspension bridge with caisson foundation, this paper mainly studies the bonding properties between underwater pre-filled aggregate grouting bed and anchorage caisson foundation. Through the test, the cohesive force of adding ordinary concrete between the anchorage caisson foundation and the grouting bed, the cohesive force of adding paper base asphalt felt between the anchorage caisson foundation and the grouting bed, and the cohesive force of adding geotextile between the anchorage caisson foundation and the grouting bed are measured, respectively. When the contact surface is concrete and geotextile, the fracture form of the specimen was analyzed by numerical simulation, and the AE variation trend of the two specimens have been studied. The results of this article can provide references for other projects.

Keywords: anchorage caisson foundation; grouting bed; cohesive force; RFPA



Citation: Geng, T.; Chen, S.; Zhao, L.; Zhang, Z. Research on Bonding Performance of Anchorage Caisson Foundation with Different Contact Surfaces and Grouting Bed. *Buildings* **2021**, *11*, 365. <https://doi.org/10.3390/buildings11080365>

Academic Editor: Abdelhafid Khelidj

Received: 1 June 2021

Accepted: 17 August 2021

Published: 19 August 2021

Publisher's Note: MDPI stays neutral with regard to jurisdictional claims in published maps and institutional affiliations.



Copyright: © 2021 by the authors. Licensee MDPI, Basel, Switzerland. This article is an open access article distributed under the terms and conditions of the Creative Commons Attribution (CC BY) license (<https://creativecommons.org/licenses/by/4.0/>).

1. Introduction

At present, the application of caisson foundation is more and more extensive, and it is used more in large and important structures such as wharves, breakwaters, and bridges. The research on the design, construction, and transportation of caisson foundation is becoming more and more developed [1–3]. However, the contact problem between the caisson foundation and the grouting bed needs to be improved. Different construction techniques and different contact surface forms will affect the bonding performance between structures [4–7].

At present, some scholars have studied the bond properties of concrete [8–11]. Liu et al. studied the bond characteristics of mortar and concrete in anchor-mortar-concrete three-phase medium by using the push-out test of mortar from concrete block [12]. Dong presented the calculation method of the maximum temperature difference that the FRP-to-concrete interface could bear, based on the presented theoretical models [13]. Zhao studied the design of field test schemes on friction and bonding properties between caisson and grouting bed [14]. Zhu et al. discovered efficient methods to improve the interfacial bonding behavior between existing concrete and attached concrete during retrofitting [15]. Yu et al. observed that pull-out peak load and corresponding wire end slippage increase with the embedment length and density of foam concrete [16]. Chiou et al. proposed a method based on large-scale geotechnical field testing [17]. It can be seen from the above discussion that there is little research on the bond performance between structural concrete and grouting bed.

Based on the Dalian Xinghai Bay Bridge Anchorage Project (Figure 1), this paper conducts in-depth experimental research on the bonding performance between the bottom of caisson and the grouting bed, which is carried out under different contact forms to obtain different bonding forces so as to provide some references for other projects.



Figure 1. Dalian Xinghai Bay Sea-crossing Bridge.

2. Model Test Plan

2.1. Specimen Production

According to the natural conditions of the construction site and the capacity of the experimental equipment, the rubble bed was used for the grouting bed. The original pool on site was used in the grouting site, the bottom of the pool was poured with concrete, and the side wall of the pool was heightened and reinforced; the size of the refurbished pool was about $15\text{ m} \times 7\text{ m} \times 1.7\text{ m}$, so that the pool's bearing capacity meets the experimental requirements, as shown in Figure 2.



Figure 2. The site of grouting bed.

The depth of the rubble bed was 1.4 m, and the stones were 8–20 cm blocks, the stones have not been graded and screened, and the particle size distribution is relatively uniform. The porosity of the rubble bed was about 30–40%, The uniaxial compressive strength of the aggregate stone was not less than 50 MPa. The fabricated reaction frame was put into the pool where the rubble bed was located in advance, as shown in Figure 3. The mortar adopted cement mortar with fluidity of $18 \pm 4\text{ S}$, and the mortar expansion rate was 0.5–1%.

The anchor caisson foundation was represented by a concrete test block with a specification of $1\text{ m} \times 1\text{ m} \times 0.45\text{ m}$, the concrete test blocks were prefabricated with C40 concrete, and a total of 18 test blocks were made, the classification of test blocks is shown in Table 1. The prepared concrete test block was placed on the rubble bed. Considering the actual situation of the site, the $1\text{ m} \times 1\text{ m} \times 1\text{ m}$ concrete weight block was superimposed on the concrete test block during the grouting period, and then the grouting work was carried out. After the grouting was completed, it is removed, as shown in Figure 4.



Figure 3. The pre-placed reaction frame.

Table 1. Test block classification table.

Cohesion	Contact Surface Category	Ordinary Concrete	Paper Base Asphalt Felt	Geotextile
	Horizontal Cohesion	Hc	Hp	Hg
	Vertical Cohesion	Vc	Vp	Vg



Figure 4. Layout of concrete test blocks.

The contact surface between the anchor caisson foundation and the grouting bed was divided into three situations: adding ordinary concrete, adding paper base asphalt felt and adding geotextile. The jack was used to apply horizontal force and vertical force, respectively, to test the horizontal bond force and vertical bond force between the anchor caisson foundation and the grouting bed under different contact surface forms, as shown in Figure 5. The jack was controlled by a specially customized electro-hydraulic servo loading system.

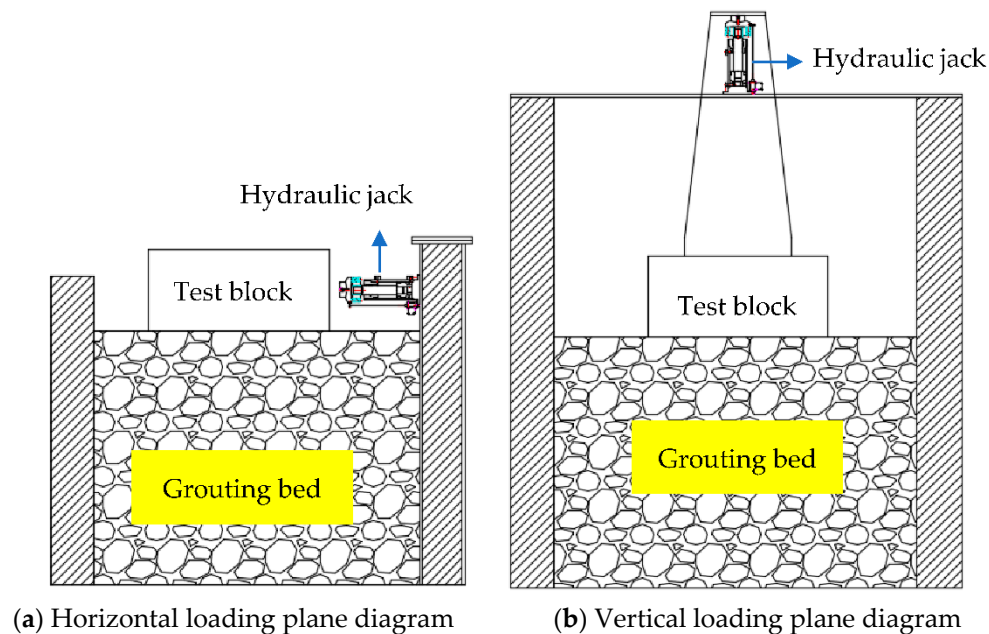


Figure 5. Schematic diagram of the distribution position of the grouting bed, concrete test block, and loading system.

2.2. Test Device

2.2.1. Horizontal Force Loading Device

A horizontal jack with a loading capacity of 200 kN fixed on the pressure-bearing column was used to apply a controllable horizontal loading force on the side of the specimen. The horizontal jack head was provided with an arc-shaped contact surface to make the test piece evenly compressed, as shown in Figure 6.



Figure 6. Horizontal loading device for simulation test.

2.2.2. Vertical Force Loading Device

The vertical force is applied to the top of the test piece by using the vertical jack with the loading capacity of 200 kN fixed on the load-bearing beam to simulate the dead weight of caisson and the upper load. Real-time monitoring of the axial force exerted by the vertical jack was performed. To ensure that the vertical jack can always be straight, so that the specimen is uniformly pulled, the vertical jack head was provided with circular contact surface, as shown in Figure 7.

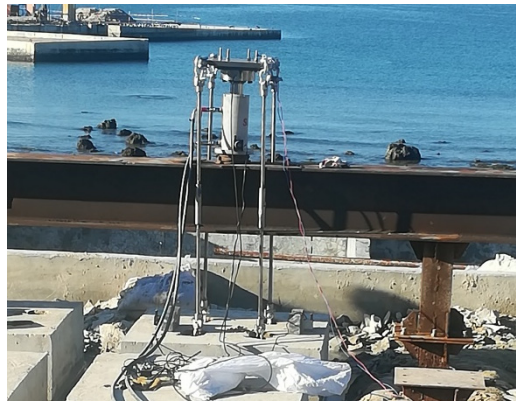


Figure 7. Vertical loading device for simulation test.

2.3. Design of Data Acquisition System

The force and displacement acting on the specimen were measured by the pressure sensor and displacement meter of the electro-hydraulic servo jack. The test system can automatically and continuously collect the measured force and displacement information, and the acquisition frequency was 10 Hz. The collected force and displacement are displayed on the control software interface in the form of curve in real time, so that the tester can grasp the change information of the test piece in time. In order to measure the displacement of the specimen, the displacement sensor was placed on the specimen for data acquisition.

2.4. Loading Scheme

After the grouting of precast grouting bed was completed, the loading frame and jack were installed, and the equipment was debugged. There are three types of contact surfaces between the anchor caisson foundation and the grouting bed: ordinary concrete, paper base asphalt felt, and geotextile.

2.4.1. Horizontal cohesive force

We only installed the horizontal jack, slowly exerted the horizontal load, and did not exert the vertical load. After the specimen started sliding horizontally, we recorded the horizontal test load value F_1 . After unloading, the load was exerted again. After the specimen slid horizontally, we recorded the horizontal test load value F_2 . It can be considered that the horizontal cohesive force was $F_h = F_1 - F_2$.

2.4.2. Vertical Cohesive Force

We only installed the vertical jack, slowly exerted the vertical load, and did not exert the horizontal load. When the specimen had a vertical displacement, we recorded the vertical load value F_3 at that time. It is considered that the vertical cohesive force was $F_v =$ the measured vertical force – the total weight of concrete test block – the initial value.

According to the test, the results of the three types of contact surfaces were analyzed and compared, and the experimental phenomena and results are summarized in combination with calculations.

3. Model Test Results

In order to eliminate the influence of errors when testing the horizontal and vertical cohesive forces, three sets of tests were performed on each contact surface, and the stress diagram of one group of specimens was analyzed.

3.1. Analysis of Horizontal Cohesive Force

The experimental loading process of adding ordinary concrete between concrete test block and grouting bed is shown in Figure 8. During the first loading, the horizontal

force of the Hc specimen reached the maximum value of 36 kN at 542 s, as shown in Figure 9a. After unloading and reloading, the horizontal force of the Hc specimen reached the maximum value of 10.7 kN at 132 s, as shown in Figure 9b. The time required for the horizontal force of the Hc specimen to reach the maximum value for the second time was 410 s earlier than the first time, and the horizontal cohesive force was 25.3 kN. It can be seen from Table 2 that the average value of the horizontal cohesive force of the Hc specimen is 25.77 kN.



Figure 8. Horizontal jack loading of Hc specimen.

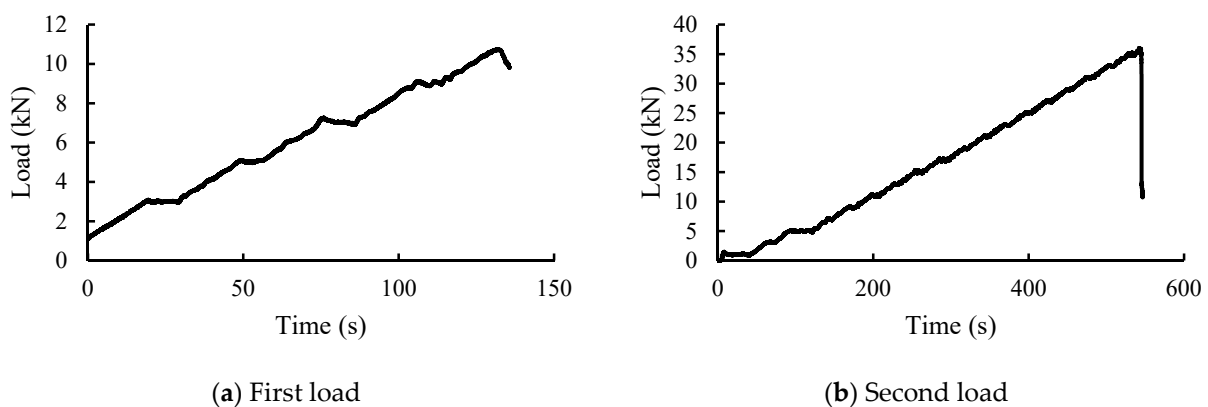


Figure 9. Loading curve of horizontal jack of Hc specimen.

Table 2. The horizontal force of specimens with normal concrete contact surface.

	Total Weight of Concrete Test Block (kN)	The First Measured Horizontal Force (kN)	Horizontal Force Measured By Reloading (kN)	Horizontal Bond Force (kN)
Hc-1	11	36	10.7	25.3
Hc-2	11	36	16	20
Hc-3	11	44	12	33
average value	11	38.67	12.90	25.77

The experimental loading process of adding paper base asphalt felt between the concrete test block and the grouting bed is shown in Figure 10. During the first loading, the horizontal force of the Hp specimen reached the maximum value of 14 kN at 264 s, as shown in Figure 11a. After unloading and loading again, the maximum horizontal force on Hp specimen reached 6.05 kN in the 85 s, as shown in Figure 11b. The time required for the horizontal force of the Hc specimen to reach the maximum value for the second

time was 179 s earlier than the first time, and the horizontal cohesive force was 7.95 kN. It can be seen from Table 3 that the average value of the horizontal cohesive force of the Hp specimen is 10.98 kN.



Figure 10. Horizontal jack loading of Hp specimen.

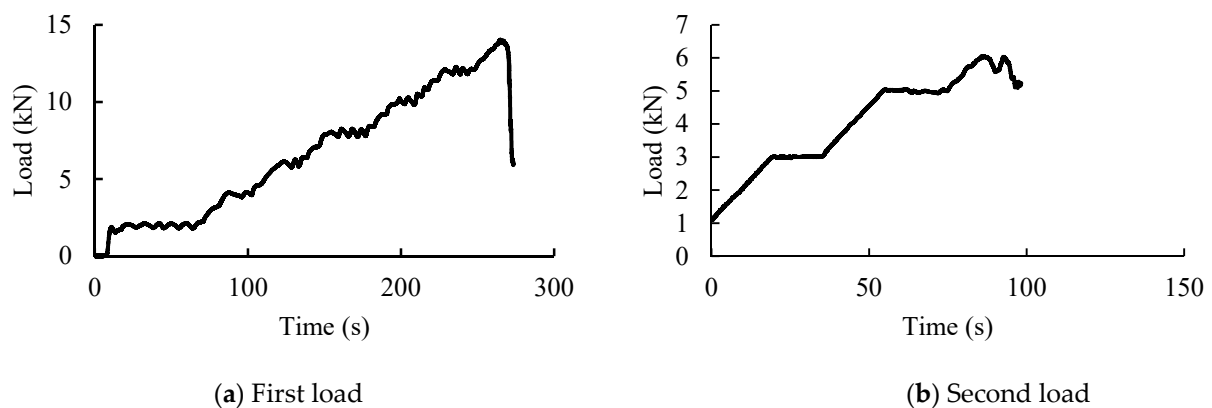


Figure 11. Loading curve of horizontal jack of Hp specimen.

Table 3. The horizontal force of the test piece when the contact surface is paper base asphalt felt.

	Total Weight of Concrete Test Block (kN)	The First Measured Horizontal Force (kN)	Horizontal Force Measured by Reloading (kN)	Horizontal Bond Force (kN)
Hp-1	11	14	6.05	7.95
Hp-2	11	20	11	9
Hp-3	11	26	20	16
average value	11	20.00	12.35	10.98

The experimental loading process of adding geotextile between the concrete test block and the grouting bed is shown in Figure 12. During the first loading, the horizontal force of the Hg specimen reached the maximum value of 12 kN at the 168 s, as shown in Figure 13a. After unloading and reloading, the horizontal force of the Hg specimen reached the maximum value of 10 kN at 127 s, as shown in Figure 13b. The time required for the horizontal force of the Hg specimen to reach the maximum value for the second time was 41 s earlier than the first time, and the horizontal cohesive force was 2 kN. It can be seen from Table 4 that the average value of the horizontal cohesive force of the Hg specimen is 4 kN.



Figure 12. Hg specimen loaded by horizontal jack.

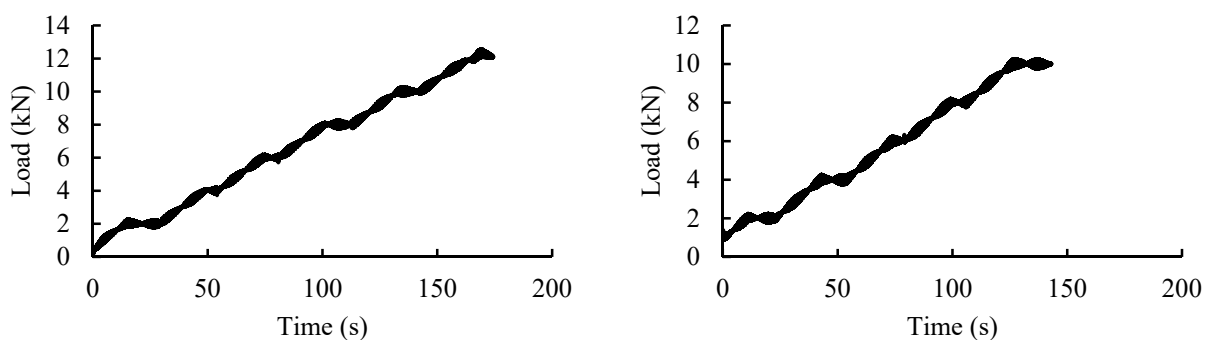


Figure 13. Horizontal jack loading curve of Hg specimen.

Table 4. Horizontal force of the specimen with geotextile on the contact surface.

	Total Weight of Concrete Test Block (kN)	The First Measured Horizontal Force (kN)	Horizontal Force Measured by Reloading (kN)	Horizontal Bond Force (kN)
Hg-1	11	12	10	2
Hg-2	11	20	12	8
Hg-3	11	14	12	2
average value	11	15.33	11.33	4.00

3.2. Analysis of Vertical Cohesive Force

The experimental loading process of adding concrete between concrete test block and grouting bed is shown in Figure 14. The vertical force of the Hg specimen reached the maximum value of 31.1 kN at 286 s, as shown in Figure 15. It can be seen from Table 5 that the average value of the vertical cohesive force of the Hg specimen is 2.71 kN.

Table 5. The vertical force of the specimen with the contact surface of ordinary concrete.

	Total Weight of Concrete Test Block (kN)	Initial Value (kN)	Load Measured Vertical Force (kN)	Vertical Bonding Force (kN)
Hc-1	11	17.2	31.0	2.8
Hc-2	11	17.5	31.0	2.5
Hc-3	11	17.18	31.1	2.92
average value	11	17.29	31.0	2.71



Figure 14. Vertical jack loading of Hc specimen.

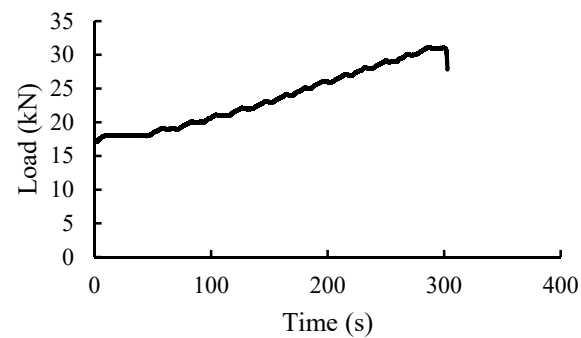


Figure 15. Vertical jack loading curve of Hc specimen.

The experimental loading process of adding paper base asphalt felt between the concrete test block and the grouting bed is shown in Figure 16. The vertical force endured by the Hp specimen reached the maximum value of 30.9 kN at 269 s, as shown in Figure 17. It can be seen from Table 6 that the average value of the vertical cohesive force of the Hp specimen is 2.13 kN.



Figure 16. Vertical jack loading of Hp specimen.

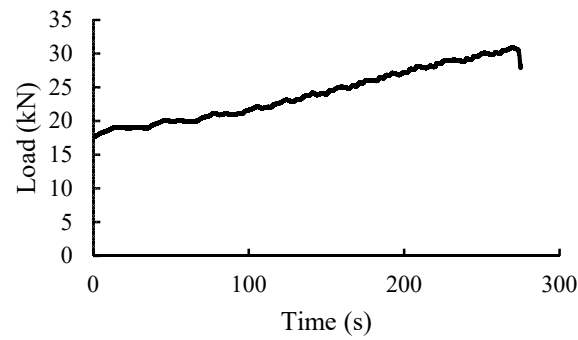


Figure 17. Vertical jack loading curve of Hp specimen.

Table 6. The vertical force of the test piece when the contact surface is paper base asphalt felt.

	Total Weight Of Concrete Test Block (kN)	Initial value (kN)	Load Measured Vertical Force (kN)	Vertical Bonding Force (kN)
Hp-1	11.8	16.8	28.4	0.6
Hp-2	11.8	17.7	30.9	2.2
Hp-3	11.8	18.3	32.9	3.6
average value	11.8	17.60	30.73	2.13

The experimental loading process of adding geotextile between the concrete test block and the grouting bed is shown in Figure 18. The vertical force of the Hg specimen reached the maximum value of 31 kN at 299 s, as shown in Figure 19. It can be seen from Table 7 that the average value of the vertical cohesive force of the Hg specimen is 4.03 kN.



Figure 18. Vertical jack loading of Hg specimen.

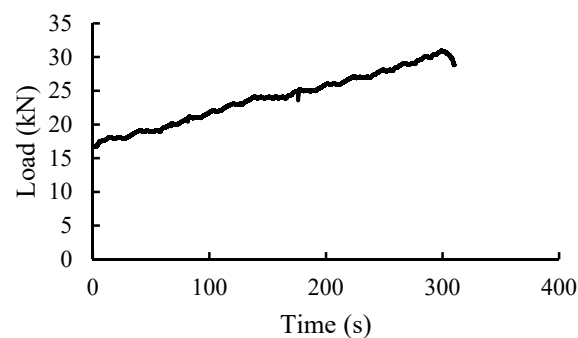


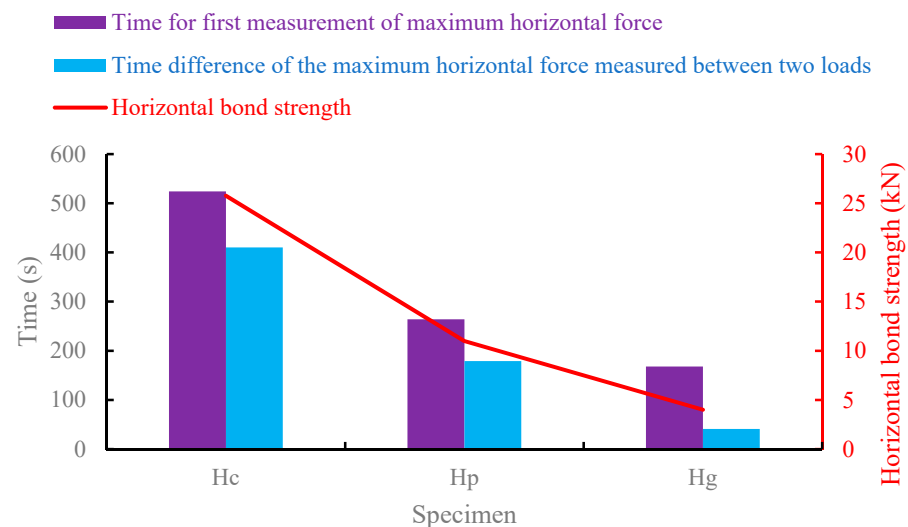
Figure 19. Loading curve of vertical jack of Hg specimen.

Table 7. Vertical force of test piece with geotextile on the contact surface.

	Total Weight Of Concrete Test Block (kN)	Initial Value (kN)	Load Measured Vertical Force (kN)	Vertical Bonding Force (kN)
Hg-1	11	18.2	34.5	5.3
Hg-2	11	16.7	31	3.3
Hg-3	11	16.5	31	3.5
average value	11	17.13	32.17	4.03

3.3. Discussion on Test Results

It can be seen from Figure 20 and Table 8 that the horizontal bearing capacity of the specimen with the contact surface of concrete was the largest, and the time required to measure the maximum horizontal bearing capacity at the first load was also the longest. The results show that the horizontal bearing capacity of the specimen with geotextile interface was the smallest, and the time required to measure the maximum horizontal bearing capacity for the first time was also the least. At the same time, the biggest time difference of the maximum horizontal bearing capacity measured by two loading was the specimen with concrete interface. The above discussion shows that the pre-filled aggregate grouting bed can provide greater horizontal cohesive force for the anchor caisson. It can be seen from Figure 21 and Table 9 that the vertical bearing capacity of the specimen with the geotextile contact surface was the largest, and the time required to load to the maximum vertical bearing capacity was also the longest, but its vertical bearing capacity was only slightly larger than that of the specimen with concrete interface.

**Figure 20.** Comparison of the horizontal bonding strength of different specimens and the time when the maximum horizontal force was measured.**Table 8.** The horizontal bonding strength of different specimens and the time when the maximum horizontal force was measured.

	Hc	Hp	Hg
Horizontal cohesive force (kN)	25.77	10.98	4
Time of maximum horizontal bearing capacity measured at the first loading (s)	524	264	168
Time of maximum horizontal bearing capacity measured by the second loading (s)	132	85	127
The time difference of the maximum horizontal bearing capacity measured by two loadings (s)	410	179	41

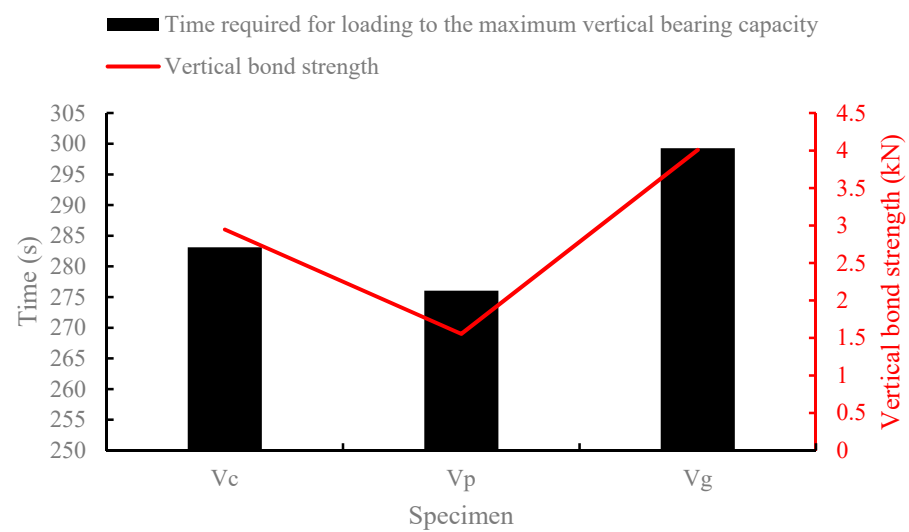


Figure 21. Comparison of the vertical bonding strength of different specimens and the time required to measure the maximum vertical bearing capacity.

Table 9. The vertical bonding strength of different specimens and the time required to measure the maximum vertical bearing capacity.

	Vc	Vp	Vg
Vertical cohesive force (kN)	2.71	2.13	4.03
Time required for loading to the maximum vertical bearing capacity (s)	286	269	299

4. Numerical Simulation Analysis

The horizontal bond strength of the specimen with concrete interface was the largest, and that of the specimen with geotextile interface was the smallest, and the difference between them was very large. In this paper, RFPA software was used to analyze in detail the fracture process of the two specimens and the change of acoustic emission during the fracture process.

4.1. Introduction to RFPA Software

Realistic Failure Process Analysis (RFPA) software is a numerical analysis tool developed based on the real failure process analysis method that can simulate the progressive failure of materials. In 1995, Professor Tang Chun'an of China developed RFPA software based on finite element theory and statistical damage theory. The software considers the non-uniformity of material properties, and deals with the failure of the element satisfying the given strength criterion, so that the numerical simulation of the failure process of non-uniform material can be realized. Because of the unique calculation and analysis method of RFPA software, it can solve the problems that most numerical simulation software cannot solve in civil engineering [18,19].

The features of RFPA software are as follows [10–23]: (1) it is assumed that the properties of the unit are approximately elastic and brittle, but because of the non-uniformity of the material, the macroscopic properties of the material may be nonlinear properties with softening relations; (2) the failure element does not have tensile capacity, but has a certain anti-extrusion capacity; (3) the non-uniformity of the material is expressed by the non-uniformity of the element mechanical parameter distribution; (4) the program treats the failed element with reduced rigidity. Through this method, physically discontinuous problems can be treated with mechanics of continuum.

4.2. Numerical Model

The lower part of the model is the grouting bed, the upper part of the model is the anchorage caisson foundation, and the middle part of the model is the interface. The force state of the numerical model is shown in Figure 22. The size of the lower part of the model is $1\text{ m} \times 1\text{ m}$, and the number of divided units is 100×100 . The size of the upper part of the model is $1\text{ m} \times 0.4\text{ m}$, and the number of divided units is 100×45 . The left and right sides and the bottom of the grouting bed are fixed, and the load is applied on the right side of the anchorage caisson foundation. The contact surface is concrete or geotextile.

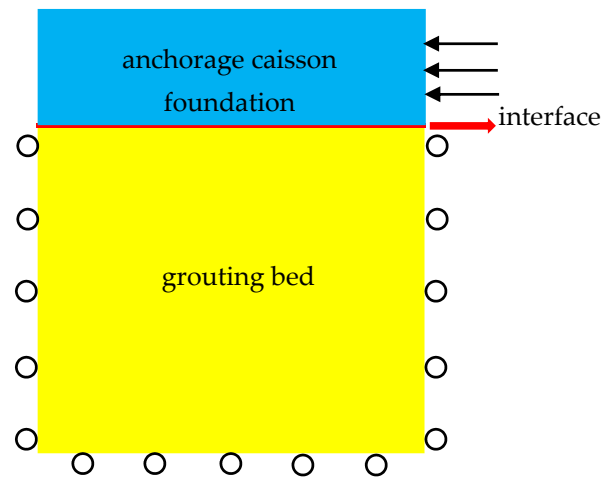
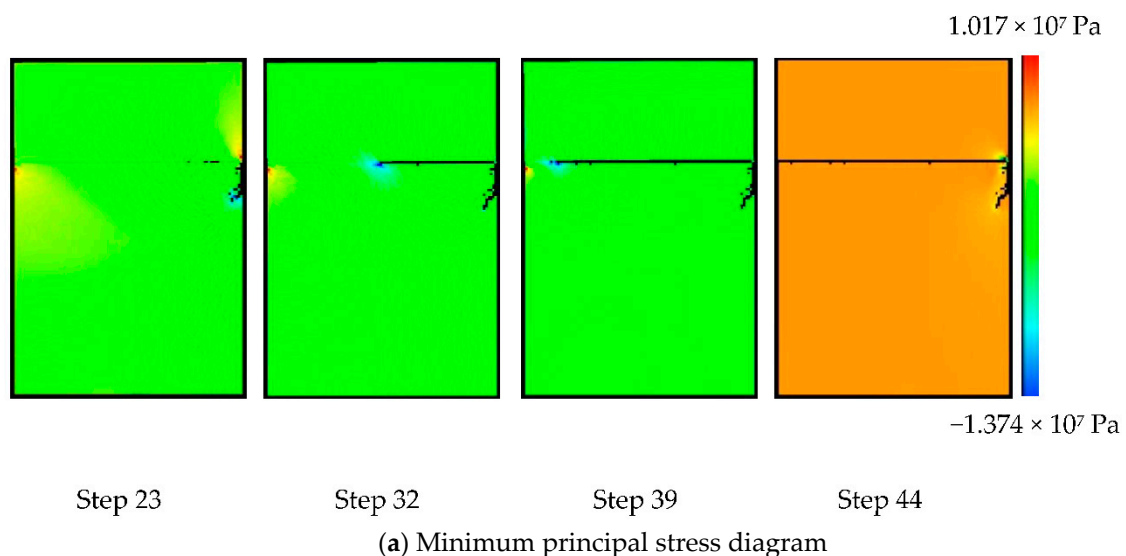


Figure 22. Numerical model.

4.3. Analysis of Numerical Simulation Results

Figures 23 and 24 are the failure stress diagrams and acoustic emission diagrams of different contact surface samples obtained from numerical experiments. Each circle in the AE diagram represents an AE event, and the size of the circle represents the relative energy or magnitude, which is proportional to the strength of the unit. The white circle represents shear failure, the red circle represents tensile failure, and the position of the circle represents the location of AE event. The black element in the stress diagram indicates the damaged element. It can be seen from the AE diagram that the failure mode of the specimens is tensile fracture whether the contact surface is concrete or geotextile, and both the numerical models are gradually broken from right to left.



(a) Minimum principal stress diagram

Figure 23. Cont.

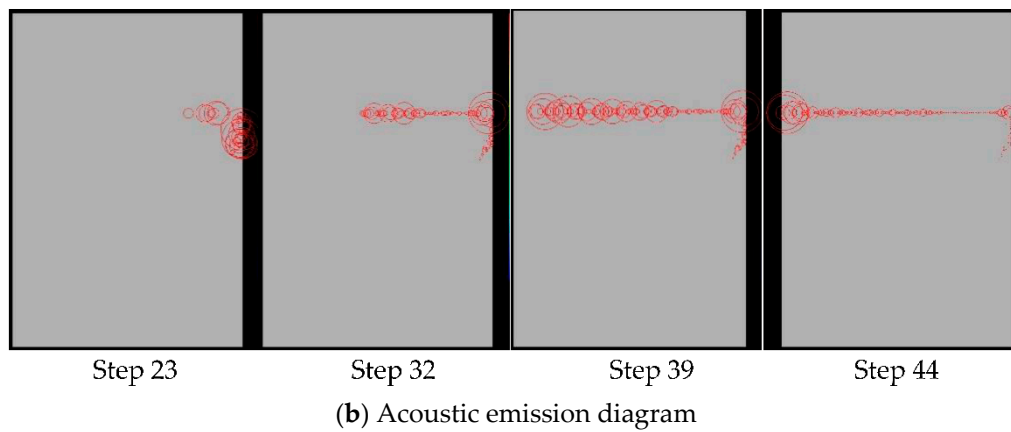


Figure 23. Failure process of specimens with concrete interface.

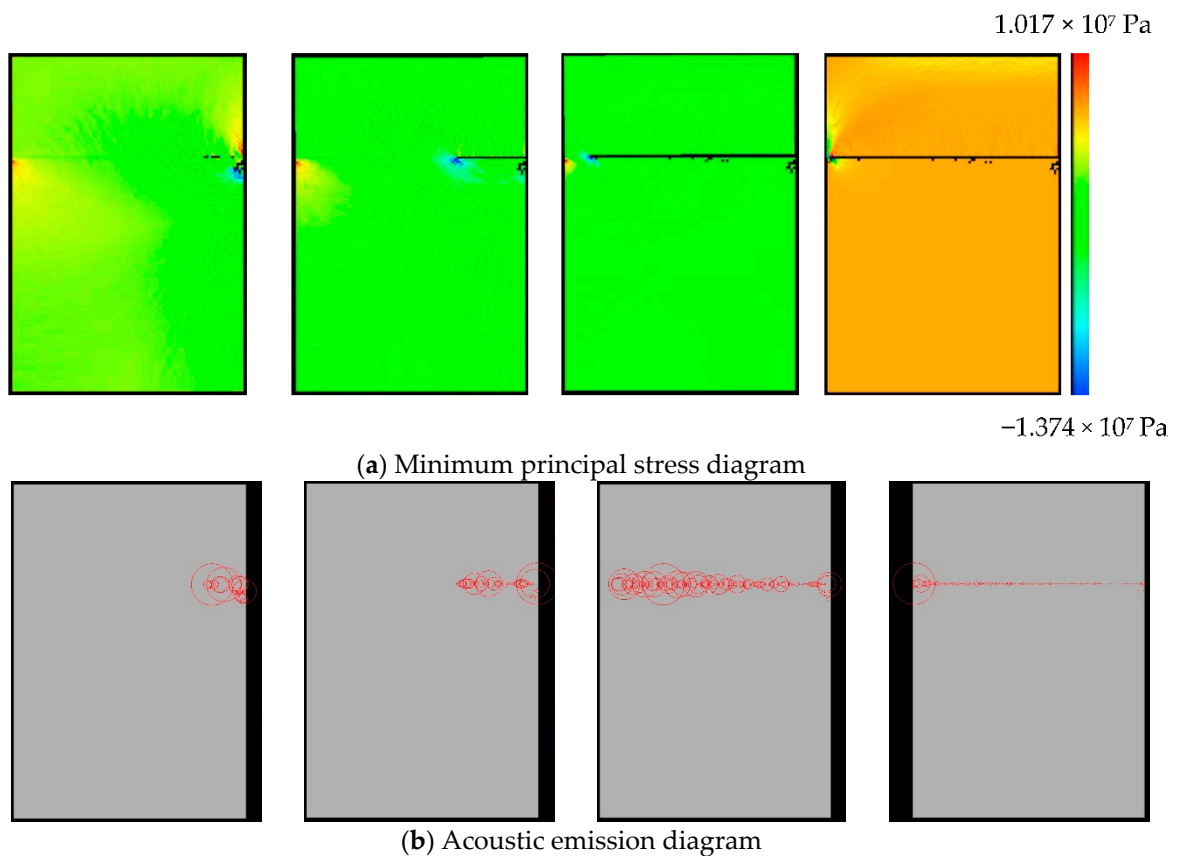
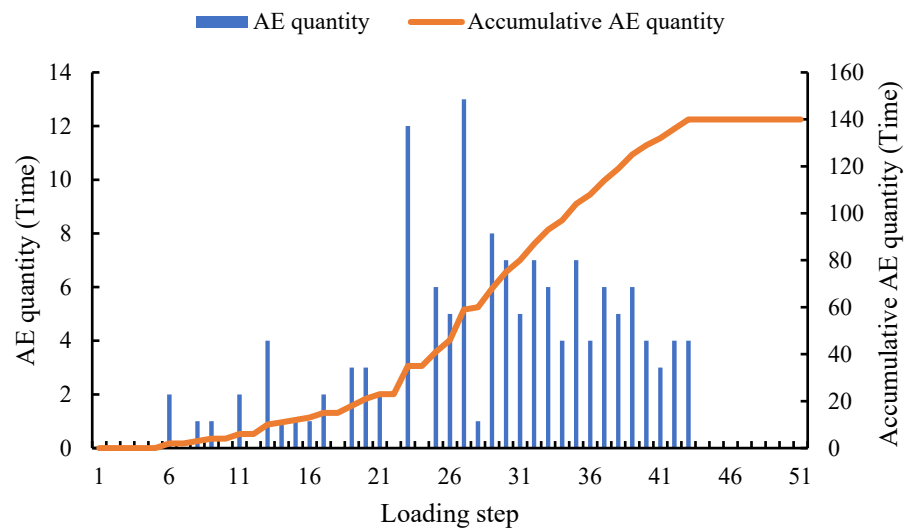
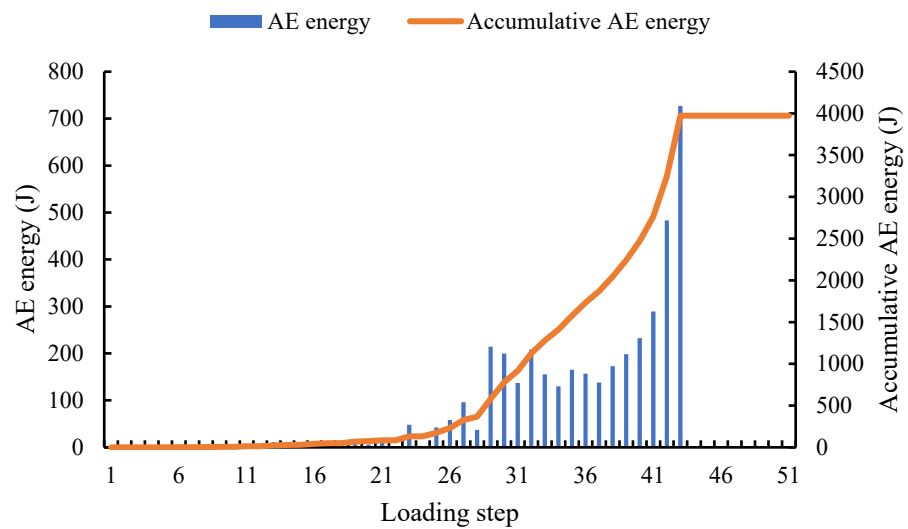


Figure 24. Failure process of specimen with geotextile interface.

As shown in Figure 25, when the contact surface is concrete, the AE quantity is higher in the middle of the loading period, and the AE quantity reached the maximum value of 13 at the 27th loading step. The accumulative AE quantity after the end of the loading is 140. The AE energy reached the maximum value of 727 J in the last loading step. The accumulative AE energy after loading is 3973.



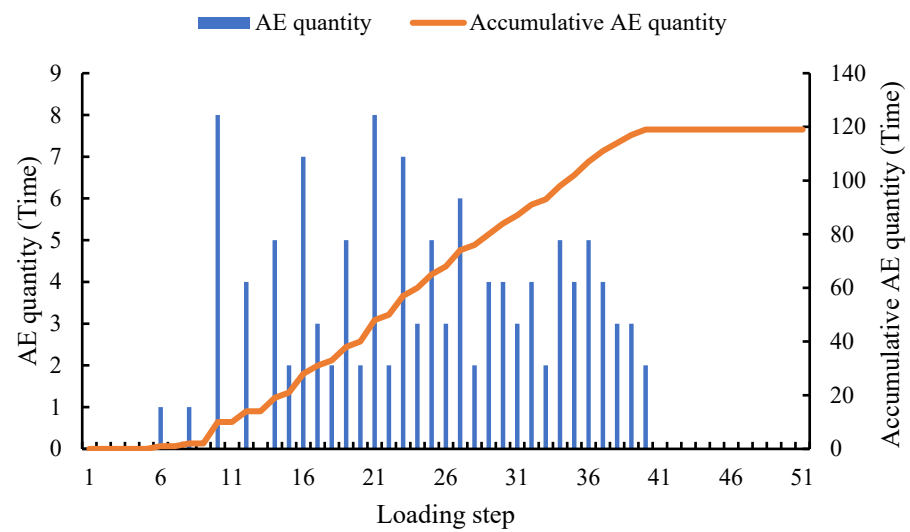
(a) AE quantity



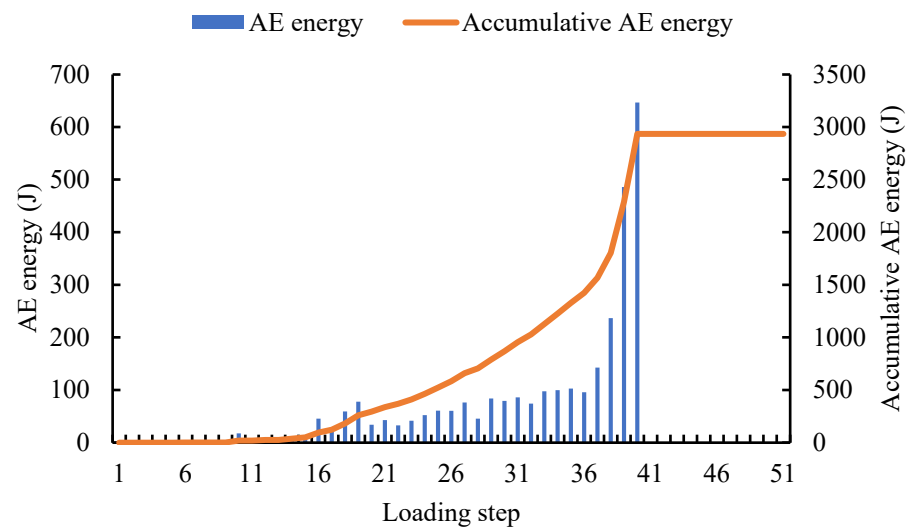
(b) AE energy

Figure 25. Acoustic emission variation trend of specimens with concrete contact surface.

As shown in Figure 26, when the contact surface is geotextile, the AE quantity is distributed discretely during the entire loading process, the AE quantity both reached the maximum value of 8 at the 10th and 21st loading steps, and the accumulative AE quantity after the end of the loading is 119. The AE energy reached the maximum value of 647 J in the last loading step. The accumulative AE energy after loading is 2935.



(a) AE quantity



(b) AE energy

Figure 26. Variation trend of acoustic emission of specimen with geotextile interface.

5. Conclusions

- (1) The pre-filled aggregate grouting bed can provide greater cohesive force for the caisson. By adding paper base asphalt felt between the caisson and the grouting bed, the pre-filled aggregate grouting bed can provide the caisson with a smaller horizontal cohesive force and a smaller vertical cohesive force. The geotextile is added between the caisson and the grouting bed, and the pre-filled aggregate grouting bed can provide the caisson with lower horizontal cohesive force and slightly larger vertical cohesive force.
- (2) The failure form of the specimen with concrete contact surface is tensile failure. When the specimen breaks, it releases more AE energy and more AE quantity, which indicates that it needs more horizontal load to make this kind of specimen break. It also shows that when the contact surface is concrete, the stability of the grouting bed and anchorage caisson is the best.
- (3) Adding ordinary concrete between the anchorage caisson foundation and the grouting bed can meet the needs of the project. The horizontal cohesive force of the specimen

with concrete contact surface was 25.77 kN, which requires more energy when the specimen ruptures.

Author Contributions: Conceptualization, T.G. and Z.Z.; methodology, T.G.; software, T.G.; validation, T.G., S.C. and L.Z.; formal analysis, S.C.; investigation, L.Z.; resources, L.Z.; data curation, T.G.; writing—original draft preparation, T.G.; writing—review and editing, T.G.; visualization, T.G.; supervision, Z.Z.; project administration, T.G.; funding acquisition, Z.Z. All authors have read and agreed to the published version of the manuscript.

Funding: This research was funded by the National Natural Foundation of China, grant number 51778108 and the APC was funded by Zhe Zhang.

Conflicts of Interest: The authors declare no conflict of interest.

References

- Kumar, N.D.; Rao, S.N. Earth pressures on caissons in marine clay under lateral loads-A laboratory study. *Appl. Ocean Res.* **2010**, *32*, 58–70. [[CrossRef](#)]
- Hu, Y.; Randolph, M.F. Bearing capacity of caisson foundations on normally consolidated clay. *Soils Found.* **2002**, *42*, 71–77. [[CrossRef](#)]
- Wen, C. Uniaxial behaviour of suction caissons in soft deposits in deepwater. *Science* **2005**, *310*, 638–642.
- Zhu, S.; Liu, J.; Chen, X.; Zhu, Z. Investigation of scour effects on the vertical bearing capacity of suction caissons considering stress history. *Mar. Georesour. Geotechnol.* **2021**, *2*, 1–9.
- Faul, G.L.; Audibert, J.; Hamilton, T.K. Using Suction Technology for Deep Installation of Structural Pipe in Deepwater. *Tech. Phys.* **1998**, *58*, 968–972.
- Sankarbabu, K.; Sannasiraj, S.A.; Sundar, V. Hydrodynamic performance of a dual cylindrical caisson breakwater. *Coast. Eng.* **2008**, *55*, 431–446. [[CrossRef](#)]
- Chen, X.; Li, Y.; Teng, B. Numerical and simplified methods for the calculation of the total horizontal wave force on a perforated caisson with a top cover. *Coast. Eng.* **2007**, *54*, 67–75. [[CrossRef](#)]
- Tayeh, B.A.; Bakar, B.A.; Johari, M.M.; Ratnam, M.M. The relationship between substrate roughness parameters and bond strength of ultra high-performance fiber concrete. *J. Adhes. Sci. Technol.* **2013**, *27*, 1790–1810. [[CrossRef](#)]
- Júlio, E.N.; Branco, F.A.; Silva, V.D.; Lourenço, J.F. Influence of added concrete compressive strength on adhesion to an existing concrete substrate. *Build. Environ.* **2006**, *41*, 1934–1939. [[CrossRef](#)]
- Momayez, A.; Ehsani, M.R.; Ramezani pour, A.A.; Rajaie, H. Comparison of methods for evaluating bond strength between concrete substrate and repair materials. *Cem. Concr. Res.* **2005**, *35*, 748–757. [[CrossRef](#)]
- Santos, P.M.D.; Júlio, E.N.B.S. Factors affecting bond between new and old concrete. *ACI Mater. J.* **2011**, *108*, 449–456.
- Liu, Y.L.; Yang, S.T.; Huang, W. Study of test method on bond performance between mortar and concrete. *Eng. Mech.* **2013**, *30*, 217–220. (In Chinese)
- Dong, K.; Hao, J.W.; Li, P. Studies on the bond performance of FRP-to-concrete interfaces under environmental temperature difference. *Eng. Mech.* **2020**, *37*, 117–126.
- Zhao, L.Q.; Hu, J.H.; Tan, Y.B. Design of Field Test Scheme on Property between Caisson and Grouting Bed. *Exp. Sci. Technol.* **2020**, *18*, 84–87.
- Zhu, Y.; Li, X.B.; Pu, Y.L. Experimental Study on the Methods to Improve Interfacial Bonding Behavior between Existing Concrete and Attached Concrete. *J. Sichuan Univ.* **2016**, *48*, 128–134.
- Yu, L.; Fu, Y.Y.; Zhang, J.; Wang, J.H. Test and simulation on pull-out behavior of steel wire in foam concrete. *J. Harbin Inst. Technol.* **2016**, *48*, 119–123.
- Chiou, J.S.; Ko, Y.Y.; Hsu, S.Y.; Tsai, Y.C. Testing and analysis of a laterally loaded bridge caisson foundation in gravel. *Soils Found.* **2012**, *52*, 562–573. [[CrossRef](#)]
- Tang, C.A. *Numerical Experiments of Rock Failure Process*; Science Press: Beijing, China, 2003. (In Chinese)
- Tang, C.A. Numerical simulation of progressive rock failure and associated seismicity. *Int. J. Rock Mech. Min. Sci.* **1997**, *34*, 249–261. [[CrossRef](#)]
- Tang, C.; Chen, F.; Sun, X.; Ma, T.; Du, Y. Numerical analysis for support mechanism of constant-resistance bolts. *Chin. J. Geotech. Eng.* **2018**, *40*, 2281–2288.
- Chen, F.; Tang, C.A.; Sun, X.M.; Ma, T.H.; Du, Y.H. Supporting characteristics analysis of constant resistance bolts under coupled static-dynamic loading. *J. Mt. Sci.* **2019**, *16*, 1160–1169. [[CrossRef](#)]
- Tang, C.A.; Kaiser, P.K. Numerical simulation of cumulative damage and seismic energy release in unstable failure of brittle Rock: Part I Fundamentals. *Int. J. Rock Mech. Min. Sci.* **1998**, *35*, 113–121. [[CrossRef](#)]
- Chen, F.; Du, Y.H.; Sun, X.M.; Ma, T.H.; Tang, C.A. Numerical experimental study on influence factors of anchoring force of constant resistance bolt. *Geomat. Nat. Hazards Risk* **2021**, *12*, 424–442. [[CrossRef](#)]